Plastic flattening of a sinusoidal metal surface

Sun, Fengwei; Van der Giessen, Erik; Nicola, Lucia

Published in:
Wear

DOI:
10.1016/j.wear.2012.08.007

Publication date:
2012

Wear 296 (2012) 672–680

Contents lists available at SciVerse ScienceDirect

Wear

journal homepage: www.elsevier.com/locate/wear

Plastic flattening of a sinusoidal metal surface: A discrete dislocation plasticity study

Fengwei Sun [a], Erik Van der Giessen [b], Lucia Nicola [a,*]

[a] Department of Materials Science and Engineering, Delft University of Technology, 2628CD Delft, The Netherlands
[b] Zernike Institute for Advanced Materials, University of Groningen, 9747 AG Groningen, The Netherlands

ARTICLE INFO

Article history:
Received 29 April 2012
Received in revised form
3 August 2012
Accepted 8 August 2012
Available online 18 August 2012

Keywords:
Contact mechanics
Rough surface
Dislocation dynamics
Surface topography
Size effect

ABSTRACT

The plastic flattening of a sinusoidal metal surface is studied by performing plane strain dislocation dynamics simulations. Plasticity arises from the collective motion of discrete dislocations of edge character. Their dynamics is incorporated through constitutive rules for nucleation, glide, pinning and annihilation. By analyzing surfaces with constant amplitude we found that the mean contact pressure is inversely proportional to the wavelength. For small wavelengths, due to interaction between plastic zones of neighboring contacts, the mean contact pressure can reach values that are about 1/10 of the theoretical strength of the material, thus significantly higher than what is predicted by simulations that do not account for size dependent plasticity. Surfaces with the same amplitude to period ratio have a size dependent response, such that if we interpret each period of the sinusoidal wave as the asperity of a rough surface, smaller asperities are harder to be flattened than large ones. The difference between the limiting situations of sticking and frictionless contacts is found to be negligible.

1. Introduction

Due to roughness, contact between two surfaces occurs primarily at the summits of the surface asperities, so that the area really affected by contact is just a small fraction of the body surface. Nevertheless, the forces generated in such a small area are responsible for most tribological phenomena, like friction and wear.

In general the surface topography is a mixture of shapes spanning different length scales and can nowadays be measured with high precision. By contrast, the change in contact area during loading is not easily measurable. Since the contact area evolves in a non-trivial way during contact, knowledge of the initial topography is of little use for determination of friction during contact [1]. Therefore, rough surface modeling can contribute to the prediction of friction by allowing to track the evolution of the area of contact as well as the contact pressure during loading.

Traditional contact mechanics models based on the work of Greenwood and Williamson [2] give an approximate evaluation of contact area and pressure for a collection of asperities, but they neglect the elastic interaction between asperities. More precise predictions can be obtained using the statistical friction models, like Persson's [3] and its modification by Müser [4], but these works mainly focus on the assumption that the flattened asperities behave elastically. The pressure predicted by such models exceeds the hardness of the material on many contacts at rather low loads. In addition to that, experimental studies of rough surface contact [5,6] indicate that the pressure in the contacts is sufficiently high for plastic deformation to take place. We therefore believe it is of interest to investigate what role plasticity really plays. Even though it might be expected that the change in contact area and pressure would depend strongly on the plastic deformation of the asperities, finite element simulations of elasto-plastic bodies with a rough surface by Pei et al. [7] seem to disprove that, and to indicate that when the material behaves plastically, self-affine surfaces with different morphology deform in a similar way. Their results also confirm the interesting finding by Gao et al. [8] that the mean contact pressure of each asperity of the surface is increased by interaction between neighboring asperities but limited to approximately twice the single asperity hardness. Gao et al. [8] account for the elastic–plastic interaction of neighboring asperities and find that this interaction hinders flattening of the surface, to the point that the true contact area converges to zero.

The purpose of this publication is to shed some light on the role of size dependent plasticity in the flattening of a rough metal surface. The roughness of the surface is strongly simplified to a sinusoidal wave function, but plasticity caused by dislocation glide is carefully computed by discrete dislocation simulations [9]. The numerical technique has so far proven successful to capture size dependent plastic behavior of isolated flat contacts [10] as

* Corresponding author. Tel.: +31 15 278 8806; fax: +31 15 278 6730.
E-mail address: l.nicola@tudelft.nl (L. Nicola).

0043-1648/$ - see front matter © 2012 Elsevier B.V. All rights reserved.
http://dx.doi.org/10.1016/j.wear.2012.08.007

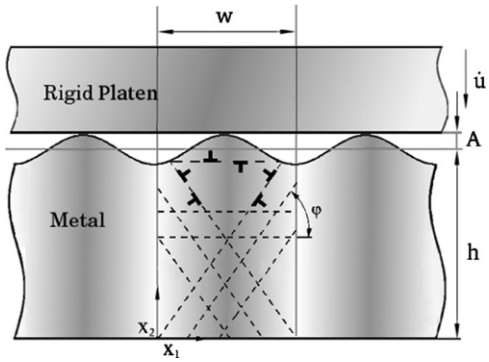

Fig. 1. Two-dimensional model of a single crystal with surface flattened by a rigid platen.

well as interplay between plasticity underneath arrays of flat contacts [11,12].

2. Formulation

The model problem is shown in Fig. 1. A rigid platen flattens the sinusoidal surface of a semi-infinite single crystal with amplitude A and wavelength w. The top surface of the crystal is described by

$$f(x_1) = h - A\cos\left(\frac{2\pi x_1}{w}\right).$$

The analysis is performed on a unit cell encompassing a full period of the surface wave and periodic boundary conditions are imposed at the right and left borders of that cell. The load is imposed by prescribing the vertical displacement of the rigid platen:

$$u_2(x_1, f(x_1)) = -\int \dot{u}\, dt, \quad x_1 \in C, \tag{1}$$

where C is the contact area, defined as the flat region of intimate contact between the flat platen and the crystal where displacement is prescribed. By regions of intimate (or true) contact we refer to sum of areas where two or more adjacent surface nodes are in contact with the platen. Outside the contact region, the top surface ($x_2 = f(x_1)$) is traction free. The traction distribution along the contact normal to the platen determines the flattening force F_n (per unit of length):

$$F_n := -\int_{x_1 \in C} \sigma_{22}\, dx_1. \tag{2}$$

Imposing boundary conditions that account for realistic interaction between surface and platen is compromised by the lack of knowledge about the friction coefficient between surfaces at such scale. Therefore we confine our study to the two limiting situations for the contact conditions:

frictionless (non-adhesive) contact :

$$\sigma_{12}(x_1, f(x_1)) = 0, \quad x_1 \in C, \tag{3}$$

sticking (adhesive) contact : $u_1(x_1, f(x_1)) = 0, \quad x_1 \in C.$ (4)

Periodic boundary conditions are imposed at the vertical sides of the unit cell,

$$u_1(w, x_2) - u_1(0, x_2) = U_1, \quad u_2(0, x_2) = u_2(w, x_2). \tag{5}$$

For crystals with sticking contacts the value of the uniform expansion U_1 is taken to be zero. This condition is necessary to fulfill the requirements that (1) the platen must be rigid and (2) the contacts stick to the platen. Note that even if the unit cell is bound to not expand, i.e. $U_1 = 0$, the lateral boundaries of the unit cell are not constrained to remain straight. For the frictionless contacts we will consider two possibilities: $U_1 = 0$ or U_1 is determined from the condition that lateral expansion of the unit cell can take place freely, since the material can slide underneath the contacts, as expressed by

$$\Sigma_{11} := \frac{1}{h}\int_0^{h-A} \sigma_{11}(x_1, x_2)\, dx_2 = 0. \tag{6}$$

We will therefore analyze three different boundary value problems that will be referred to as follows:

- Sticking-Constrained (S-C): no slip at the contacts, Eq. (4), and no overall lateral strain, i.e. $U_1 = 0$;
- Frictionless-Constrained (F-C): no friction at the contact, Eq. (3), and no overall strain, $U_1 = 0$;
- Frictionless-Unconstrained (F-U): no friction at the contact and no overall stress $\Sigma_{11} = 0$ (free expansion of the unit cell), Eq. (6).

A comparison between results obtained with the first two boundary conditions, S-C and F-C, will give insight in the importance of the friction conditions at the contact. Contrasting the last two conditions, F-C and F-U, will instead tell us if the material that can slide underneath the contact will behave differently if given the possibility to expand. For further reference the boundary conditions studied are summarized in Table 1.

The simulations follow the formulation for discrete dislocation plasticity by Van der Giessen and Needleman [9]: the solution for the dislocated crystal is given by the linear composition of the closed-form elastic solution for the dislocations in an infinite medium and the numerical correction for the image fields. The latter is calculated by the finite element method. The mesh is made of very fine square elements at the surface of the crystal, to correctly capture the contact area and the dislocation fields, the mesh is coarser at the bottom of the crystal, where there are no dislocations.

The crystal is taken to have the elastic properties of aluminum: Young's modulus $E = 70$ GPa and Poisson's ratio $\nu = 0.33$. Following Rice [13] the FCC crystal is modeled in two dimensions by considering three potentially active slip systems with orientations $\varphi = 0^\circ$, 60° and 120°. The spacing between slip planes in the crystal is $200b$, where b is the Burgers vector of magnitude $b = 0.25$ nm. At the beginning of the simulation, the crystal is dislocation free and it contains a given density of obstacles and dislocation sources distributed randomly on the slip planes in the crystal. The obstacles represent small precipitates in the material as well as forest dislocations present as a consequence of previous plastic deformation. When the resolved shear stress at the dislocation sources is sufficiently high, edge dislocations are generated. The mean nucleation strength for the sources is taken to be $\overline{\tau}_{\mathrm{nuc}} = 50$ MPa, with 20% standard deviation. The time span necessary for nucleation of a dislocation dipole, t_{nuc}, is taken to be 10 ns. The values used in these simulations are the outcome of a quantitative comparison with experimental results in [14].

Table 1
Contact conditions and conditions on the horizontal expansion U_1 of the unit cell.

Contact-expansion	Contact conditions	Expansion conditions
S-C	Eq. (4)	Eq. (5); $U_1 = 0$, $\Sigma_{11} \neq 0$
F-C	Eq. (3)	Eq. (5); $U_1 = 0$, $\Sigma_{11} \neq 0$
F-U	Eq. (3)	Eq. (6); $U_1 \neq 0$, $\Sigma_{11} = 0$

3. Effect of boundary conditions

Two crystals with average height $h=12\ \mu m$ and surface amplitudes $A=0.2\ \mu m$ and $A=0.8\ \mu m$ are flattened by $u=0.04\ \mu m$. The spacing between contacts w, which corresponds also to the width of the unit cell, is taken to be constant and initially rather wide, i.e. $w=10\ \mu m$. The density of dislocation sources and obstacles is $\rho=30\ \mu m^{-2}$. The simulations are performed using the three different combinations of boundary conditions defined in Table 1: sticking-constrained (S-C), frictionless-constrained (F-C) and frictionless-unconstrained (F-U). The flattening force and the corresponding true contact area during flattening are compared in Fig. 2a and b, respectively. The curves for sticking (S-C) and frictionless (F-C) contacts are very close to each other. A larger difference emerges between constrained (F-C) and unconstrained (F-U) crystals. From this observation we conclude that the nature of the contact itself, be it frictionless or sticking, does not affect the flattening of the surface. Instead, flattening is affected by the extent to which the material is free to expand laterally underneath the contacts or constrained to maintain the same width in between contacts. The influence of lateral boundary conditions (constrained or unconstrained) does not depend on surface amplitude. At a flattening depth of 0.04 μm for $A=0.2\ \mu m$ the measured force for unconstrained crystals is 15% smaller than that for constrained crystals, their contact area is 9% smaller. For $A=0.8\ \mu m$, the difference in force is 17% and the difference in contact area is 8%.

For the crystal with smaller amplitude, we choose a representative realization and show the distribution of the displacements in x_1-direction together with the dislocations at final depth (in Fig. 3). The figure confirms that the flattening under frictionless contacts occurs partly by lateral expansion of the material. Also, the figure gives further evidence that the difference in contact conditions is not significant, cf. Fig. 3a vs b, but that only the possibility of expansion affects the deformation mode, Fig. 3c. The distribution of displacement in x_2 direction for the same crystals is shown in Fig. 4. It is clearly seen in this figure that material in the crystal with constrained boundary conditions (S-C and F-C) piles up in the vicinity of the contact areas (see Fig. 4a and b), whereas pile-up does not occur in the F-U crystal (Fig. 4c) due to lateral expansion.

It is important to note that even though the virgin surface is smooth and the platen is rigid, the surface does not remain smooth. This is illustrated by the surface profiles in Fig. 5 at flattening depths $u=0.02$ and $0.04\ \mu m$. We observe that the contact area for all amplitudes and contact conditions evolves in a discontinuous way during flattening. This behavior is caused by the steps that are left when dislocations glide out of the free surface. The protruding parts of those displacement steps can create new contact with the rigid platen, while other parts will remain untouched. Therefore, the true contact area is the sum of distinct patches of contact and is significantly smaller than the apparent contact area would be (if measured from the first contacting point to the last one). The exit of dislocations is a stochastic process, so that different realizations show a different local evolution of the true contact area. The observation (cf. from Figs. 5a and 2b) that the contact area for the constrained crystal is slightly larger than that for the unconstrained crystal is not specific for the realization shown in Fig. 5 but is characteristic of all six realizations studied. The larger contact area in

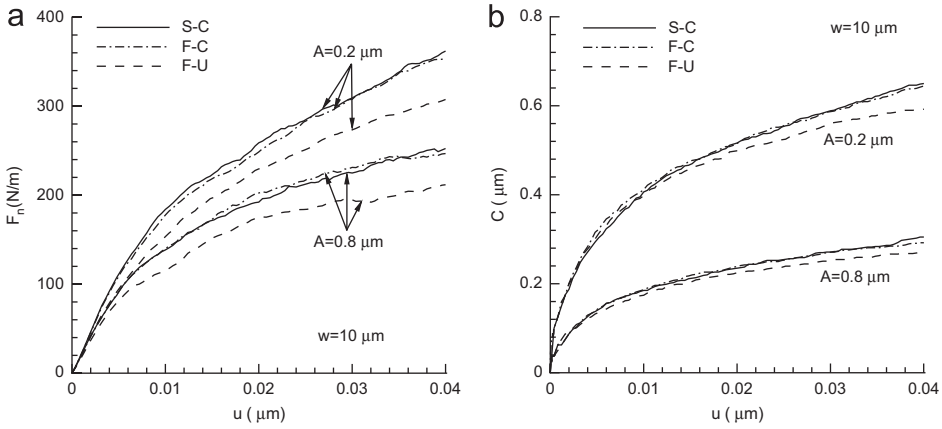

Fig. 2. (a) Force versus depth and (b) contact area evolution for S-C, F-U and F-C crystals for $A=0.2$ and 0.8 μm. Each curve represents the average of different realizations, i.e. different initial distributions of sources and obstacles strengths and locations.

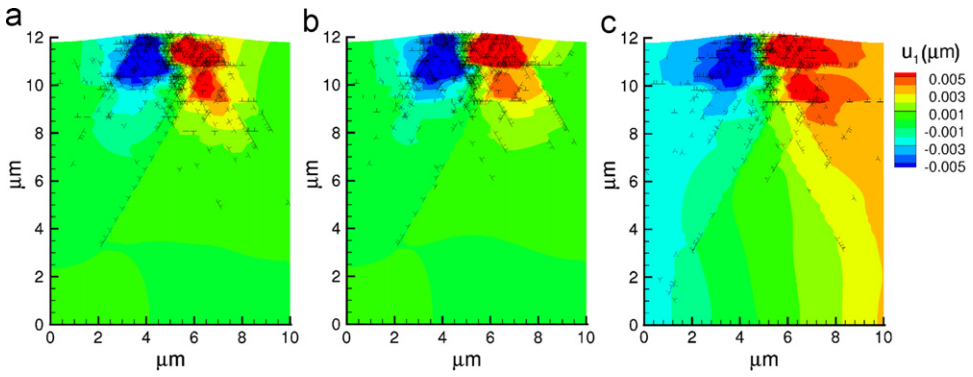

Fig. 3. The distribution of horizontal displacement u_1 for the crystal with amplitude $A=0.2\ \mu m$ under (a) S-C, (b) F-C and (c) F-U contacts at the depth of 0.04 μm.

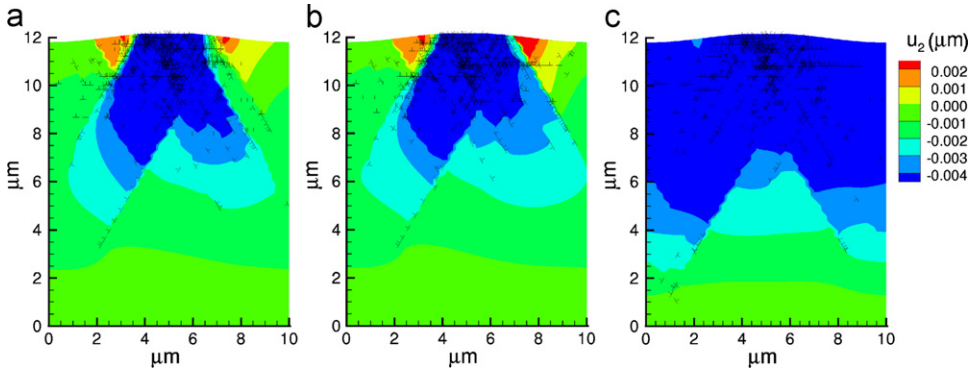

Fig. 4. The distribution of vertical displacement u_2 for the crystal with amplitude $A=0.2$ μm at the depth of 0.04 μm for various boundary conditions: (a) S-C (b) F-C and (c) F-U.

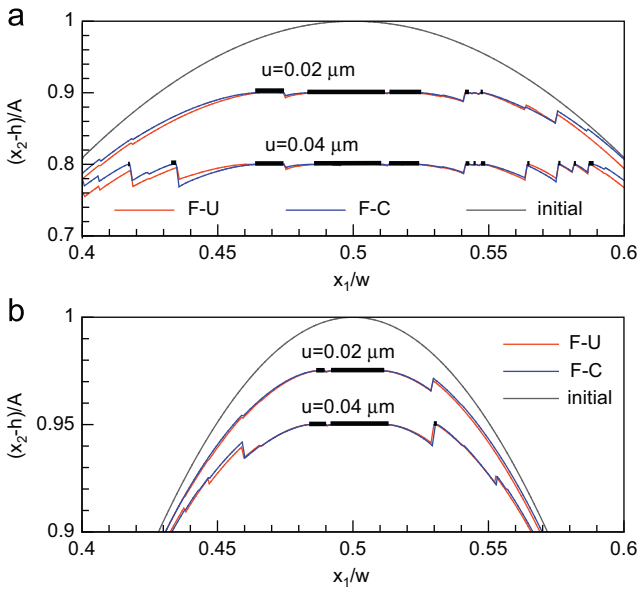

Fig. 5. Surface profile in the contact region for constrained and unconstrained crystals at the flattening depths of 0.02 μm and 0.04 μm for amplitudes (a) $A=0.2$ μm and (b) $A=0.8$ μm. Black segments indicate the areas of true contact with the platen.

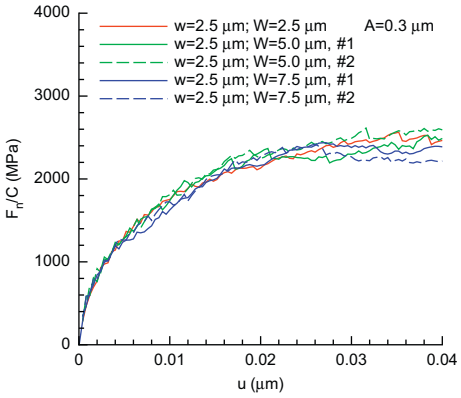

Fig. 6. Flattening force versus depth for crystals with period $w=2.5$ μm with unit cell of size $W=w$, $2w$ and $3w$. The labels #1 and #2 indicate realizations with different locations of dislocation sources.

constrained crystals can be attributed to the presence of material pile ups, see Fig. 4a and b, that help the formation of new contact regions.

The simulations reported on so far are for unit cells that encompass only a single wave of surface. When the unit cell width is small, the statistical variation of dislocation and sources locations is also small. To explore the effect of a larger source sampling, simulations are performed for unit cells of width W containing two or three wave periods w. The corresponding pressure–displacement curves in Fig. 6 show that the mean contact pressure is not affected: the difference between these curves is smaller than the difference between curves obtained by simulations with identical unit cells but with a different location of dislocation sources (indicated in the figure by #1 and #2). Therefore in the rest of the paper we will perform simulations only for $W=w$.

4. Effect of surface shape A/w

Flattening the sinusoidal surface of a single crystal is a problem that involves several lengths: the period w and amplitude A of the surface, the height of the crystal h and the average spacing between dislocation sources $L_{ave}=1/\sqrt{\rho_{nuc}}$. If the source density is large enough to ensure that sufficiently many dislocations are nucleated when needed, the source spacing L_{ave} will not affect the results and the behavior will depend only on w, A and h.

We here investigate the effect of changing period w on surface pressure while keeping the other lengths constant: $A=0.3$ μm, $h=12$ μm and $L_{ave}=0.18$ μm. We will confine attention to crystals with frictionless contacts and constrained unit cells. Fig. 7a shows how the mean contact pressure,

$$P_m=\frac{1}{C}\int_{x_1\in C}\sigma_{22}\,dx_1, \tag{7}$$

where C is the true contact area, increases with decreasing period for surfaces with $w=1.875$, 2.5, 3.75, 7.5 and 15 μm. This trend is expected and in agreement with the elastic behavior of the crystal, since the contact fraction, C/w, increases with increasing period. Anyhow, since our goal is to study the behavior of the surface and not of the whole crystal under flattening, we plot in Fig. 7b the mean contact pressure P_m, normalized by AE^*/w, as a function of the flattening strain $\varepsilon_d=(d_0-d)/d_0$ (note that this parameter is similar to that introduced by Persson [15]), but differs in the normalization distance d_0 rather than the *rms* of the original surface). Here, d is the separation distance between the platen and the average height of the crystal surface, d_0 the initial separation distance and $E^*=E/(1-\nu^2)\approx 78.5$ GPa. Normalizing the pressure by AE^*/w allows us to obtain elastic curves that are almost overlapping, by that facilitating comparison between surfaces with different w. Also, these curves do not contain any dependence on the crystal height h, as shown in Fig. 7b by comparing results for crystals with $h=12$ μm and $h=24$ μm.

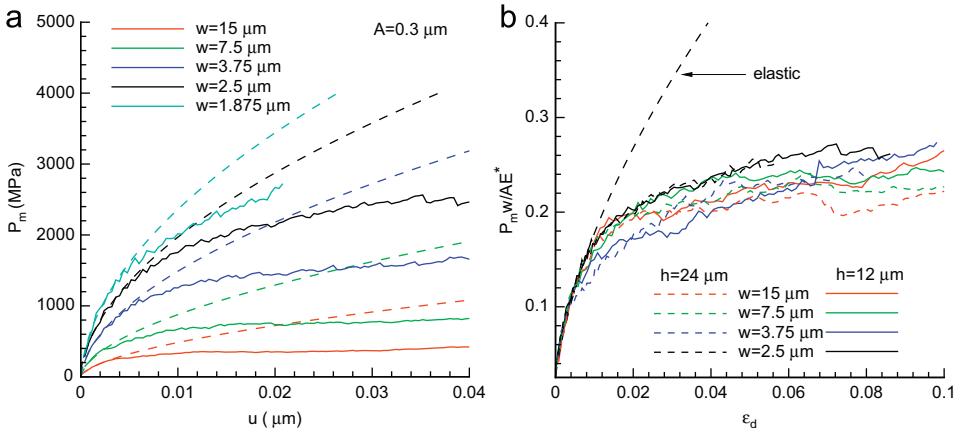

Fig. 7. (a) Mean contact pressure as a function of flattening depth for different periods w and constant amplitude $A=0.3$ μm. The dashed curves indicate the elastic solutions. (b) Normalized mean contact pressure versus ε_d for various periods w and two different crystal heights.

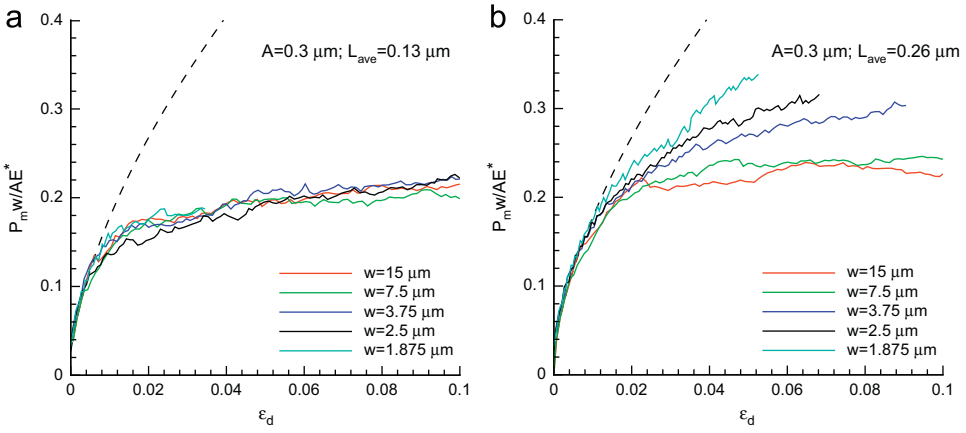

Fig. 8. Mean contact pressure normalized by AE^*/w for different dislocation source spacings (a) $L_{ave}=0.13$ μm, (b) $L_{ave}=0.26$ μm. The dashed curves indicate the elastic solution.

By looking at Fig. 8a we can see that the plastic response of the surfaces of crystals with various w are very close to each other, deviation from elasticity occurring at about $\varepsilon_S=0.007$.

If we want to approach the limit of continuum plasticity we can repeat the simulations in Fig. 7 with a higher density of dislocation sources. We observed that decreasing the spacing between dislocation sources below $L_{ave}=0.13$ μm does not affect the results; for $L_{ave}=0.13$ μm we obtain curves that are almost overlapping (see Fig. 8a). The plastic response of the surface does not additionally depend on w, i.e. P_m is just inversely proportional to w, meaning that plasticity in the asperities is size independent. For a twice as large dislocation source spacing, though, i.e. four times as large dislocation density, results are significantly different and reveal a clear size dependence: surfaces with smaller w are harder than surfaces with a larger w (see Fig. 8b). Thus, if $w/L_{ave}<3.75/0.26\approx 15$ and for a constant A, the onset of plasticity is still inversely proportional to w but plastic curves have considerably different strain hardening. For a better look at what happens locally for different wavelengths w, Fig. 9a and b shows the stress state and the dislocation structures for $w=15$ and 2.5 μm for the smallest source spacing, $L_{ave}=0.13$ μm. Note that the stress level of the lower part of the two crystals is different because the nominal pressure differs by a factor 6 (cf. Fig. 8a). The state in the subsurface regions is very different, with the crystals with smaller period having a very high density of dislocations everywhere in the top ~ 2 μm of the crystal. By contrast, there is an isolated plastic zone underneath the contact in the crystal with larger period. This translates into the dislocation density being higher for the smaller w, see Fig. 9c, for both source densities tested. The fact that the dislocation density increases with decreasing period, together with the dislocation distribution in Fig. 9b, indicates that the plastic zones underneath neighboring asperities interact progressively more as the period is decreased, thus giving rise to progressively larger mean contact pressures. Our expectation is that these results will still be valid in the case of a microcrystalline material, based on the following considerations: (a) if the grain size is much larger than the contact spacing most grain boundaries will be located outside of the plastic zones and therefore not affect the results; (b) if the grain size is comparable to contact spacings, the grain boundaries that are in the plastic zone will affect it by hindering dislocation motion. The hindering of dislocation glide has two opposite effects on contact pressure: on the one hand it decreases it by reducing the interaction between plastic zones, on the other hand it enhances contact pressure because plasticity in the crystal is reduced.

The detailed pressure distribution on the contacts is given in Fig. 10. Surfaces with larger periods make discontinuous contact with the flat platen (see also Fig. 5), while surfaces with smaller periods are characterized by a single contact region. As a consequence of the fact that the contact area is patchy, the distribution of contact pressure on surfaces with larger roughness periods is highly non-uniform: the larger region of contact has a much lower average stress than the smaller contact patches around it, which are subjected to very high stress peaks (see Fig. 10). The average mean contact pressure found

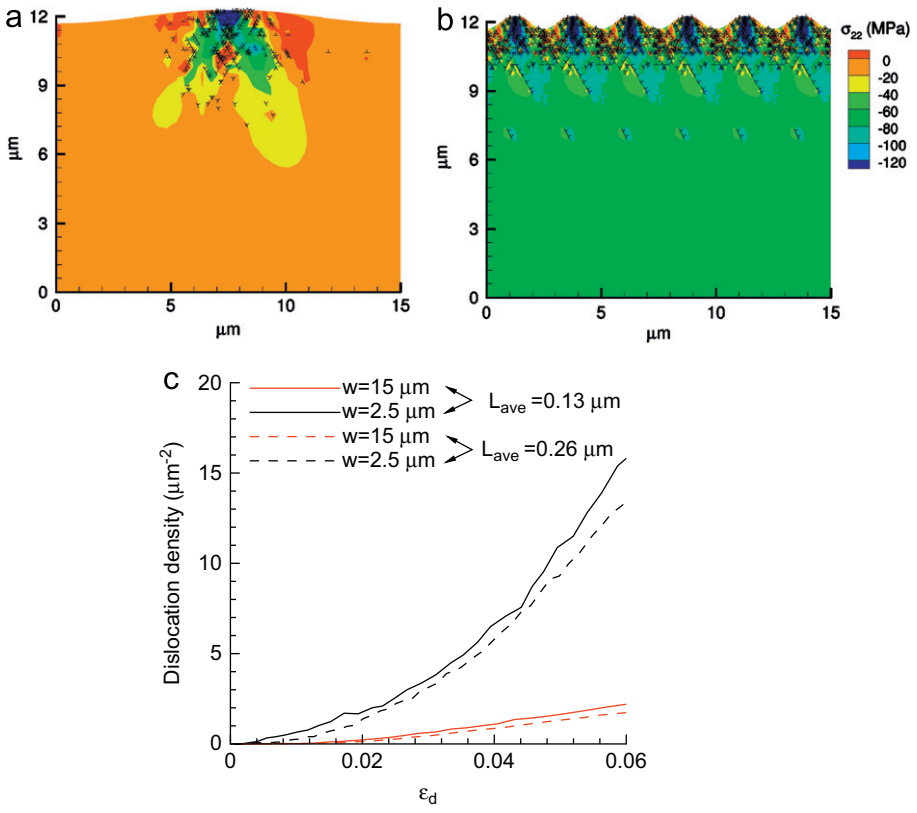

Fig. 9. Stress state and dislocation distribution at $\varepsilon_d = 0.056$ for crystals with amplitude $A = 0.3$ μm, surface periods (a) $w = 15$ μm and (b) $w = 2.5$ μm (six copies of the unit cell plotted to facilitate the comparison) and source spacing $L_{ave} = 0.13$ μm. (c) Dislocation density during flattening for different source spacings.

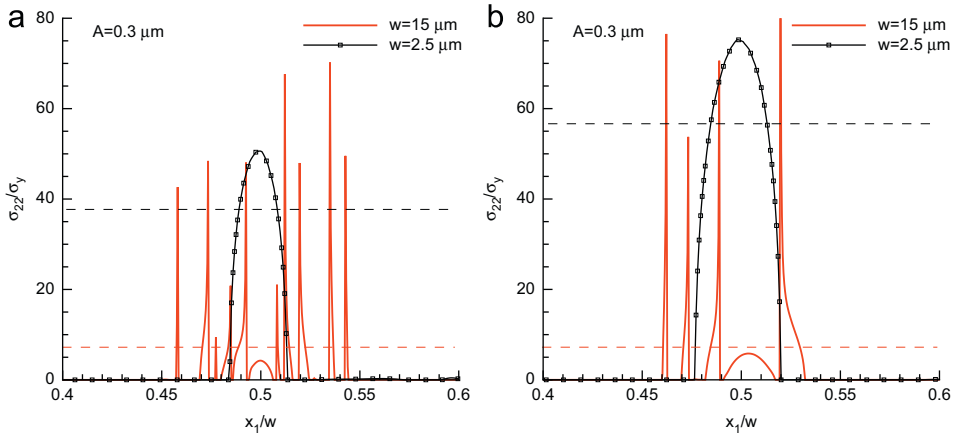

Fig. 10. Contact pressure distribution for surfaces with different periods at $\varepsilon_d = 0.056$ when the source spacing is (a) $L_{ave} = 0.13$ μm and (b) $L_{ave} = 0.26$ μm.

on each asperity for $w = 15$ μm is about $6\sigma_y$[1] for the large source density and about $7\sigma_y$ for the low source density. For $w = 2.5$ μm the mean contact pressure is remarkably higher, i.e. $P_m \approx = 38\sigma_y$ for the large source density and $P_m \approx = 56\sigma_y$ for small source density. These findings are in contrast with what is predicted by classical plasticity simulations [7,16], according to which contacts are continuous and the mean contact pressure on a single asperity is limited to about $6\sigma_y$. While the discontinuous nature of contact in our simulations and the corresponding high stress concentrations can be unrealistically high due to the fact that the simulations are two dimensional, surface steps due to plastic activity are real so that patchy contact is likely to occur in reality.

So far we have varied the surface shape A/w by changing w and keeping A constant. Next, we carry out simulations for various amplitudes of the sinusoidal wave, i.e. $A = 0.2$, 0.4, 0.6 and 0.8 μm, by keeping the period fixed at $w = 10$ μm.

Fig. 11a shows the mean contact pressure normalized by (AE^*/w) as a function of ε_d for various source spacings. Just as for the previous simulations, the elastic solutions overlap, but the onset of plasticity depends on amplitude. Increasing the average spacing between sources from $L_{ave} = 0.13$ μm to 0.26 μm, i.e. decreasing the source density, results in a further increase of the relative difference in the onset of plasticity.

In order to clarify how the onset of yield depends on amplitude at constant period and on period at constant amplitude, we here define the yield pressure P_{my} as the intersection between the $P_m w/AE^*$ versus ε_d curve and the corresponding elastic curve offset by $\varepsilon_S = 0.2\%$ (in the same spirit as the usual definition of the

[1] $\sigma_y \approx 50$ MPa for a single crystal with the same material properties as those of the crystals here considered under uniform compression.

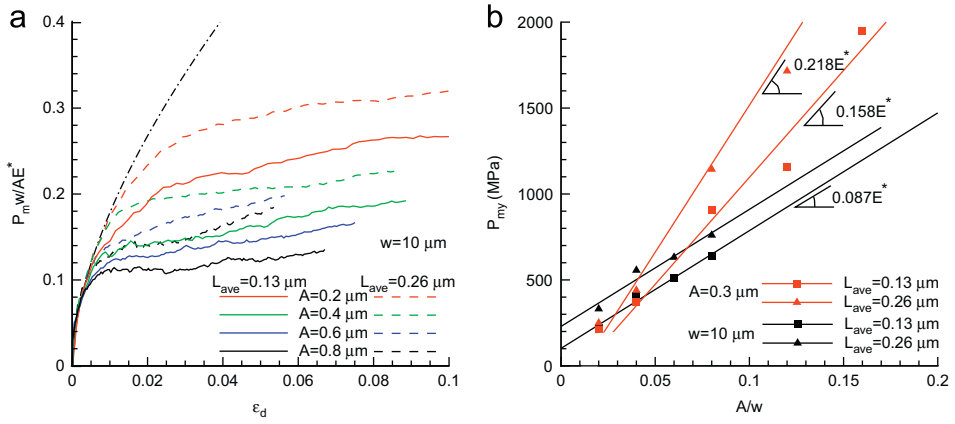

Fig. 11. (a) Normalized mean contact pressure as a function of ε_d for varying amplitudes on crystals with $L_{ave}=0.26$ μm or $L_{ave}=0.13$ μm. (b) Yield pressure for surfaces with various amplitudes and constant period, $w=10$ μm (black symbols) and with various periods but constant amplitude, $A=0.3$ μm (red symbols). Results are reported for small and large source spacing, and each data point is the average over six realizations. Lines are linear fits through the data points for the same source densities. (For interpretation of the references to color in this figure caption, the reader is referred to the web version of this article.)

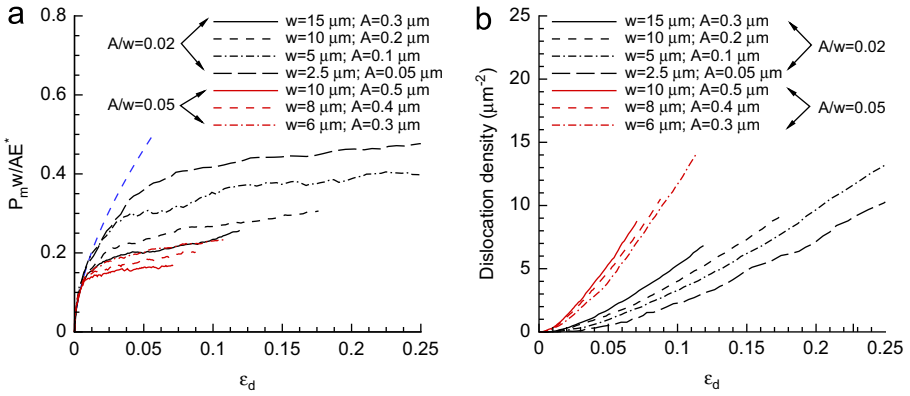

Fig. 12. (a) Mean contact pressure normalized by AE^*/w and (b) residual dislocation density versus ε_d for amplitude-to-period ratios 0.02 and 0.05, with source spacing $L_{ave}=0.13$ μm. (For interpretation of the references to color in this figure caption, the reader is referred to the web version of this article.)

0.2% yield stress in macroscopic plasticity). All the results for yield pressure obtained in this and the previous section have been compiled in Fig. 11b as a function of A/w. As previously noticed, the yield pressure at constant amplitude is inversely proportional to period, but we now also observe that the constant of proportionality increases with the source spacing. Even though we know from Fig. 11a that the surface yield pressure is not proportional to amplitude, i.e. the deviation from the elastic curve does not occur at the same $P_m w/AE^*$, the yield values extracted from Fig. 11a, as shown in black in Fig. 11b, vary linearly with A/w with a slope $0.087E^*$. If the source density is decreased the surface becomes harder, but the constant of proportionality does not change. The interesting observation in this figure thus is that if we compare surfaces with the same A/w, i.e. with the same root mean square slope, $\nabla h_{rms}=\sqrt{2}\pi A/w$, the yield pressure P_{my} is not unique, but depends on the specific choice of w and A. This signifies a size effect which we will investigate in more detail in the coming section.

5. Size dependence at constant shape A/w

In this section we compare the behavior of surfaces that have the same amplitude-to-period ratio A/w, but have various values for A and w. Specifically, we perform simulations for waves with $A/w=0.02$ with periods $w=2.5$, 5, 10 and 15 μm and for $A/w=0.05$, with periods $w=2.5$, 6, 8 and 10 μm.

Fig. 12a shows the mean contact pressure as a function of ε_d. The blue dashed line represents the corresponding elastic solution. If we interpret each period of the sinusoidal wave as the asperity of a rough surface, the results show that the plastic deformation of asperities is size dependent: for a given amplitude-to-period ratio, the pressure required to flatten a smaller asperity is larger than for a larger asperity. The larger mean contact pressure for the smaller asperity is partly due to fewer dislocations being nucleated in the crystal as shown in Fig. 12b. In order to get further insight in the origin of this, Fig. 13 shows the stress distribution and dislocation structure inside crystals with $A/w=0.05$ at $\varepsilon_d=0.056$. The plastic zone increases with increasing asperity size (i.e. increasing amplitude A and period w). Correspondingly, the dislocation density decreases (see Fig. 12b). The size dependence seems therefore to be caused by limited availability of dislocations underneath the smaller contact areas, which indeed is seen in Fig. 13.

6. Conclusions

Two dimensional simulations are performed to investigate the flattening of a sinusoidal surface with the discrete dislocation plasticity method. Three limiting situations have been

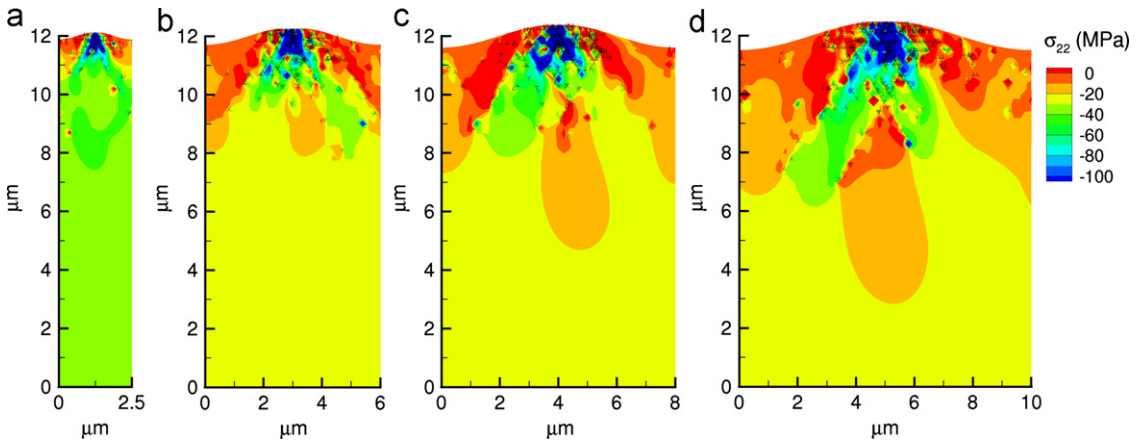

Fig. 13. Stress distribution σ_{22} for F-C crystals with constant ratio $A/w=0.05$ at $\varepsilon_d=0.056$ for different wavelengths (a) $w=2.5$ μm, (b) $w=6$ μm, (c) $w=8$ μm and (d) $w=10$ μm.

considered: the contacts are perfectly sticking (S-C), frictionless (F-U), frictionless but constrained to not expand laterally (F-C). Results have shown that:

- for sinusoidal surfaces of any period and amplitude, the contact conditions, i.e. frictionless or sticking, do not affect the flattening force nor the mean contact pressure during flattening;
- on the contrary, results depend on whether or not the material is free to expand laterally underneath the contacts. Such dependence is not affected by surface shape. If the material is constrained (which is a more reasonable assumption if we consider the constraint that the crystal would be subjected to from the material in the in-plane direction):
  - a larger force is needed to flatten the surface to a given depth;
  - a larger contact with the flattening body is achieved;
  - material pile up appears in the free surface region close to the contact.

By analyzing surfaces with various A/w we found that,

- for surfaces with constant amplitude:
  - the mean contact pressure increases with decreasing period. The mean contact pressure can reach values up to about $40\sigma_y$, thus significantly higher than what is predicted by simulations that do not account for size dependent plasticity [16];
  - the mean contact pressure is inversely proportional to period at any strain as long as the source spacing is small enough;
  - a threshold period-to-average source spacing of about 15 is found, below which it becomes even more difficult to flatten the sinusoidal surface due to additional strain hardening caused by limited source availability underneath the contacts and by plastic interaction of the asperities;
  - the yield pressure P_{my} is inversely proportional to period for all source spacing tested; the constant of proportionality is larger for larger source spacings.
- for surfaces with constant period:
  - the yield pressure can be approximated as being proportional to amplitude. The same proportionality constant $0.087E^*$ holds for small and large source spacings.
- A size dependent response is found for crystals with surfaces with the same amplitude-to-period ratio, with smaller asperities being more difficult to be deformed plastically to the same strain. As a consequence, the curves that describe the relation between load and contact area and between load and separation distance are non-unique for a given A/w, but depend on the specific choice of A, w.
- As a consequence of the fact that the area of intimate contact is discontinuous, the distribution of contact pressure is highly non-homogeneous: the larger region of contact underneath the asperity has a much lower average stress than the smaller contact regions around it, which are characterized by a very high stress concentration.

It is noteworthy that these results aim at underlying the importance of size dependent plasticity in contact mechanics but cannot straightforwardly be extended to the plastic contact between two rough surfaces. When two rough surfaces are brought into contact and plastically deform, the behavior is generally more complex than in the case of a rough surface flattened by a platen. Size dependent behavior of the asperities on both surfaces complicates matters even further.

Acknowledgment

This research was carried out under Project number MC2.06282 in the framework of the Research Program of the Materials innovation institute M2i (www.m2i.nl).

References

[1] Y. Zhang, E. Van der Giessen, L. Nicola, Discrete dislocation simulations of the flattening of nanoimprinted surfaces, Modelling and Simulation in Materials Science and Engineering 18 (2010) 034006-1–17.
[2] J.A. Greenwood, J.B.P. Williamson, Contact of nominally flat surfaces, Proceedings of the Royal Society of London A 295 (1966) 300–319.
[3] B.N.J. Persson, Theory of rubber friction and contact mechanics, Journal of Physics and Chemistry 115 (2001) 3840–3861.
[4] M.H. Müser, Rigorous field-theoretical approach to the contact mechanics of rough elastic solids, Physical Review Letters 100 (2008) 055504-1–4.
[5] J.H. Dietrich, B.D. Kilgore, Imaging surface contacts: power law contact distributions and contact stresses in quartz, calcite, glass and acrylic plastic, Tectonophysics 256 (1996) 219–239.
[6] R.S. Dwyer-Joyce, B.W. Drinkwater, A.M. Quinn, The use of ultrasound in the investigation of rough surface interface, ASME Transactions on Journal of Tribology 123 (2001) 8–16.
[7] L. Pei, S. Hyun, J.F. Molinari, M.O. Robbins, Finite element modeling of elasto-plastic contact between rough surfaces, Journal of the Mechanics and Physics of Solids 53 (2005) 2385–2409.
[8] Y.F. Gao, A.F. Bower, Elastic–plastic contact of a rough surface with Weierstrass profile, Proceedings of the Royal Society of London A 462 (2006) 319–348.
[9] E. Van der Giessen, A. Needleman, Discrete dislocation plasticity: a simple planar model, Modelling and Simulation in Materials Science and Engineering 3 (1995) 689–735.

[10] V.S. Deshpande, A. Needleman, E. Van der Giessen, Discrete dislocation plasticity analysis of static friction, Acta Materialia 52 (2004) 3135–3149.
[11] L. Nicola, A.F. Bower, K.-S. Kim, A. Needleman, E. Van der Giessen, Multi-asperity contact: a comparison between discrete dislocation and crystal plasticity predictions, Philosophical Magazine 88 (2008) 3713–3729.
[12] L. Nicola, A.F. Bower, K.-S. Kim, A. Needleman, E. Van der Giessen, Surface versus bulk nucleation of dislocation during contact, Journal of the Mechanics and Physics of Solids 55 (2007) 1120–1144.
[13] J.R. Rice, Tensile crack tip fields in elastic–ideally plastic crystals, Mechanics of Materials 6 (1987) 317–335.
[14] L. Nicola, Y. Xiang, J.J. Vlassak, E. Van der Giessen, A. Needleman, Plastic deformation of freestanding thin films: experiments and modeling, Journal of the Mechanics and Physics of Solids 54 (2006) 2089–2110.
[15] B.N.J. Persson, Relation between interfacial separation and load: a general theory of contact mechanics, Physical Review Letters 99 (2007) 125502-1–4.
[16] Y.F. Gao, A.F. Bower, K.-S. Kim, L. Lev, Y.T. Cheng, The behavior of an elastic–perfectly plastic sinusoidal surface under contact loading, Wear 261 (2006) 145–154.